Resonance Raman scattering in Si at elevated temperatures

A. Compaan* and H. J. Trodahl†
Max-Planck-Institut für Festkörperforschung, Heisenbergstrasse 1, D-7000 Stuttgart 80, Federal Republic of Germany
(Received 2 September 1983)

We have studied the resonance behavior of the Raman susceptibility for the 520-cm^{-1}, Γ'_{25}, phonon of Si from 1.8 to 3.7 eV with sample temperatures from 300 to 915 K. Both Stokes and anti-Stokes data have been obtained with thirteen cw argon- and krypton-laser lines and extracavity frequency doubling of the 752.5-nm Kr line. All data were corrected for absorption, solid-angle, and reflectivity effects using recent ellipsometric data of Jellison and Modine over a similar temperature range. The data show clearly the temperature-dependent broadening and shift ($dE/dT = -3.7\times10^{-4}$ eV/K) of the E'_0E_1 resonance. The modulus of the frequency derivative of the complex dielectric constant provides a good approximation to the Raman susceptibility when shifted higher by about one-half the phonon frequency. Resonance effects on Stokes and anti-Stokes ratios are examined carefully and related to recent Raman measurements of temperature during pulsed-laser annealing.

INTRODUCTION

Phonon Raman scattering in semiconductors is mediated by electronic transitions and consequently shows strong resonance behavior in the vicinity of direct band-to-band transitions.[1] In the case of silicon the lowest direct gap is the E'_0,E_1 gap at $\sim$3.4 eV at room temperature arising from transitions along an extended region in the Λ direction (E_1), where the valence and conduction bands are nearly parallel and from transitions at the Γ point (E'_0). The resonance Raman behavior near this region has previously been studied at room temperature by Renucci *et al.*[2] These results and a number of similar studies of other semiconductors have shown that often the resonance enhancement of the Raman susceptibility is closely related to the frequency derivative of the complex optical dielectric constant $|d\epsilon/d\omega|$ as expected from a classical description of Raman scattering.[1] However, several details of the resonance structure observed by Renucci *et al.* corresponded rather poorly to structures in $|d\epsilon/d\omega|$ as inferred from existing independent absorption and reflectivity data.

Recently the resonance Raman data have received renewed scrutiny because of the need to correct Stokes- to anti-Stokes-intensity ratios for resonance effects before a lattice temperature may be inferred. Stokes- to anti-Stokes-intensity ratios obtained under pulsed-laser annealing conditions in Si have generated intense controversy[3] because the pulsed Raman results of two independent groups appear to indicate lattice temperatures no higher than 450 °C during the anneal process.[4–6] (Prevailing opinion in the field of pulsed-laser annealing holds that the lattice undergoes thermal melting at 1412 °C.[3])

The less-than-completely-satisfying agreement between calculated and observed resonance behavior[2] together with the interest in the use of Raman scattering as a diagnostic for transient lattice temperature measurements (e.g., during laser annealing) forms a strong motivation for this study of resonance behavior as a function of lattice temperature. In addition, however, the fact that Jellison and Modine[7] have recently reported new ellipsometric measurements of the complex dielectric constant of Si *at elevated temperatures* affords us a unique opportunity to make the absorption, reflectivity, and solid-angle corrections necessary to obtain the Raman susceptibility with good accuracy from the raw Raman data. Furthermore, the high-temperature ellipsometric data permit the comparison of Raman susceptibility with $|d\epsilon/d\omega|$ over an extended temperature range.

In this study we have obtained the resonance behavior of the 520-cm^{-1}, Γ'_{25}, Raman line of pure Si over the range of photon energies from 1.8 to 3.7 eV, using available cw lines from Ar and Kr lasers and using extra-cavity frequency doubling of the 752.5-nm Kr line to fill one gap in the coverage. We have studied both Stokes and anti-Stokes signals for all lines and covered the temperature range from 300 to 915 K. The observed Stokes- to anti-Stokes-intensity ratios at known sample temperatures allow us to obtain directly the "correction factor" needed to infer lattice temperatures from the Raman ratio without reference to independent absorption and reflectivity measurements. Finally the data yield accurate numbers for the shift and broadening of the E'_0,E_1 gap with temperature to compare with the E'_0 temperature shift that has recently been calculated by Allen and Cardona.[8]

THE RAMAN SUSCEPTIBILITY χ''_S

In the typical Raman experiment using photon-counting electronics one measures the scattered photon rate R_s per unit solid angle Ω for an incident-laser irradiance I_L. The scattering rate inside the scattering medium can be written as

$$\frac{dR_S}{d\Omega}=\frac{I_L}{\hbar\omega_L}\frac{d\sigma}{d\Omega}\ . \tag{1}$$

Note that $I_L/\hbar\omega_L$ is just the flux of incident photons per unit area inside the scattering medium. Equation (1) may

be taken as a definition of the quantum differential scattering cross section $d\sigma/d\Omega$.

This differential scattering cross section can then be related to a volume-independent "Raman susceptibility,"[1]

$$\chi_s''=\frac{d\chi'}{d\xi}=V^{1/2}\frac{d\chi}{d\xi}\ ,$$

where χ is the susceptibility, and ξ is the normal coordinate of the appropriate phonon mode. Thus one obtains for Stokes Raman scattering

$$\frac{d\sigma}{d\Omega}=\frac{\hbar\omega_L\omega_S^3V\eta_S}{(4\pi)^2 2c^4\omega_0\eta_L}\,|\,\epsilon_L\epsilon_S\chi_S''\,|^2[n(\omega_0)+1]\ , \tag{2}$$

where V is the scattering volume, η_S and η_L are the indices of refraction at the scattered (ω_S) and the laser (ω_L) frequencies, respectively, ϵ_L and ϵ_S are the light polarization unit vectors, and $n(\omega_0)$ is the phonon-occupation factor for the Raman mode of frequency ω_0. The indices of refraction enter because of the fact that the susceptibility is defined in terms of electric field amplitudes E, and because the irradiance is given by $I=2\epsilon_0 c\eta E^*E$, where c is the speed of light in vacuum.[9] Note that, following Cardona [Ref. 1, Eqs. (2.47)–(2.50)], we have used a volume-independent Raman susceptibility in distinction from Hayes and Loudon [cf. Ref. 9, Eq. (1.71)]. But following Ref. 9, we have explicitly included the fact that the scattering is inelastic in defining the quantum cross section, and thus the usual ω^4 of power cross sections is replaced by $\omega_L\omega_S^3$ (cf. Ref. 1, p. 37). In addition, for economy of notation, we have suppressed the tensor character of χ_S'' and vector character of the polarization unit vectors ϵ_L and ϵ_S.

It is usually not the scattering cross section $d\sigma/d\Omega$ which is of interest in resonance Raman measurements, but rather the Raman susceptibility χ_S''. (Frequently $V\chi_S''$ or $v\chi_S''$, where v is the primitive cell volume, has wrongly been termed the "Raman cross section." To avoid confusion, we shall use Raman susceptibility for χ_S'' throughout this paper.) In terms of χ_S'' the differential scattering rate inside a strongly absorbing scattering medium is given by

$$\frac{dR_S}{d\Omega}=\frac{\omega_S^3P_L\eta_S}{(\alpha_L+\alpha_S)\eta_L}\frac{n(\omega_0)+1}{32\pi^2c^4\omega_0}\,|\,\epsilon_L\epsilon_S\chi_S''\,|^2\ , \tag{3}$$

where the product VI_L has been replaced by $P_L/(\alpha_L+\alpha_S)$, which is appropriate for a backscattering configuration in strongly absorbing scattering media for which $(\alpha_L+\alpha_S)^{-1}$ is much less than the crystal thickness. Here P_L is the incident laser power inside the crystal and $\alpha_L(\alpha_S)$ is the absorption coefficient of the incident (scattered) light.

The experimentalist normally measures *outside the crystal* the scattering rate R_S' and the laser power P_L', and the collection solid angle $\Delta\Omega'$ is usually held constant *outside* the crystal. Thus the *external* scattering rate R_S' is given by

$$R_S'=\left[\frac{T_ST_LP_L'\omega_S^3}{(\alpha_L+\alpha_S)\eta_L\eta_S}\right]\left[\frac{\Delta\Omega'[n(\omega_0)+1]}{32\pi^2c^4\omega_0}\right]|\,\epsilon_L\epsilon_S\chi_S''\,|^2\ . \tag{4}$$

Here T_S and T_L are the irradiance transmission coefficients, $T=1-r$, where r is the irradiance reflectivity, at the scattered and incident frequencies, and we have used $\Delta\Omega'\cong\eta_S^2\Delta\Omega$. For our collection aperture of $f/1.8$ this last approximation yields an error of less than 2% even with the largest value of n ($n=6.8$) in this experiment.

For anti-Stokes scattering the expression is identical to Eq. (4) when all S-subscripted variables are evaluated at the anti-Stokes frequency except that (1) the term involving the phonon population, $n(\omega_0)+1$, becomes simply $n(\omega_0)$ and (2) the Stokes Raman susceptibility χ_S'' must be replaced by the anti-Stokes susceptibility, χ_{AS}''. In this respect, however, a simple time-reversal invariance argument[9,10] shows that in thermal equilibrium the anti-Stokes susceptibility at the laser frequency ω_L is equal to the Stokes Raman susceptibility for the frequency $\omega_L+\omega_0$, i.e.,

$$\chi_{AS}''(\omega_L)=\chi_S''(\omega_L+\omega_0)\ . \tag{5}$$

We use this relationship to obtain for each laser frequency a second set of values for χ_S'' upshifted by one optic phonon energy, $\hbar\omega_0$.

It has previously been shown[1,2] that the Raman susceptibility, $\chi_S''=d\chi'/d\xi$, can be approximated by the frequency derivative of the complex susceptibility. The rationale for this approximation is easily found in the case of so-called "two-band" or intraband contributions to the Raman process.[1] For silicon it appears that in addition the strongest "three-band" or interband scattering term behaves similar to the two-band term because of the small spin-orbit splitting of the valence band.[11] Thus we shall invoke the spirit of this approximation to compare our measured Raman susceptibility squared with ellipsometric measurements of the quantity $|\,d\chi/d\omega\,|^2\sim|\,d\epsilon/d\omega\,|^2$, where ϵ is the complex dielectric constant. We shall discuss the microscopic origin of the Raman susceptibility and the above approximation in the discussion section as we examine the comparison between the Raman and ellipsometric data.

EXPERIMENTAL

The Raman data were obtained in an approximate backscattering geometry with the incident and reflected laser beam at 45° to the sample normal. Scattered light was collected with a 50-mm focal length quartz lens, $f/1.7$, giving a magnification of 6 at the spectrometer. Quartz Suprasil optics were also used for focusing to an elliptical spot roughly 500×50 μm^2 on the sample. Spectrometer entrance and exit slits were operated at 0.50 and 1.0 mm, respectively, in order to accept the entire irradiated sample image and to integrate the spectral line (resolution equal to 5 Å). Slight broadening of the Raman line was evident at the two highest temperatures for the $\lambda=676.4$ and 530.9 nm data. Peak heights were corrected in these cases to give the line integral. Collection system throughput (optics, spectrometer, and phototube) was calibrated with a 3200-K tungsten-halogen lamp and checked by scattering from CaF_2 over the full range of wavelengths. We have chosen to rely on spectrometer calibration and careful laser power measurements rather than normalizing, e.g., to CaF_2 because the CaF_2 linewidth becomes very

large at high temperatures and the phonon frequency ($\sim$300 cm^{-1}) is quite different from that of Si ($\sim$520 cm^{-1}). Power measurements were obtained with a Coherent Radiation model 210 thermopile detector except at λ=376.25 nm. Here the power of $\sim$0.35 mW was measured by a photodiode whose calibration around 376 nm was independently checked against the thermopile detector.

The nominally pure Si(100) sample was mounted in a copper oven with an evacuated quartz enclosure. Temperature control was typically $\pm$2 K, and for the three highest temperatures the sample temperature was directly checked from the sample black-body radiation measured by the spectrometer at several wavelengths. The input laser polarization was selected to yield a scattered polarization appropriate for the highest spectrometer sensitivity. The incident laser power was kept below 100 mW to avoid sample-heating effects.

CORRECTIONS

The observed photocount rate is given by eR_S', where R_S' is the scattering rate of Eq. (4), and e is the relative collection efficiency calibrated as described above. The

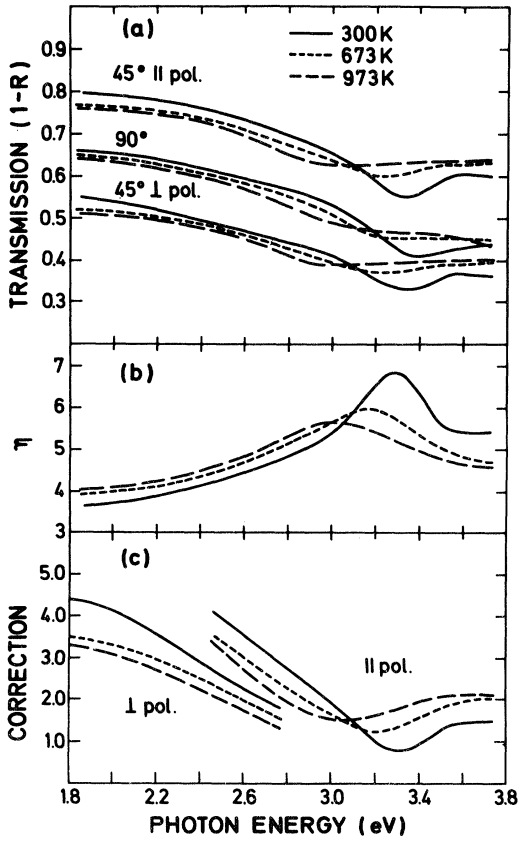

FIG. 1. Frequency dependence of transmission coefficients for normal and 45° incidence, of index of refraction η and of combined correction. The indicated correction is $160T_LT_S/\eta_L\eta_S$, where T_L (T_S) is the transmission coefficient at 45° (normal) incidence and η_L (η_S) is the index of refraction at the incident (scattered) frequency. The multiplicative factor is chosen for convenience in plotting. Curves based on optical functions of Ref. 7.

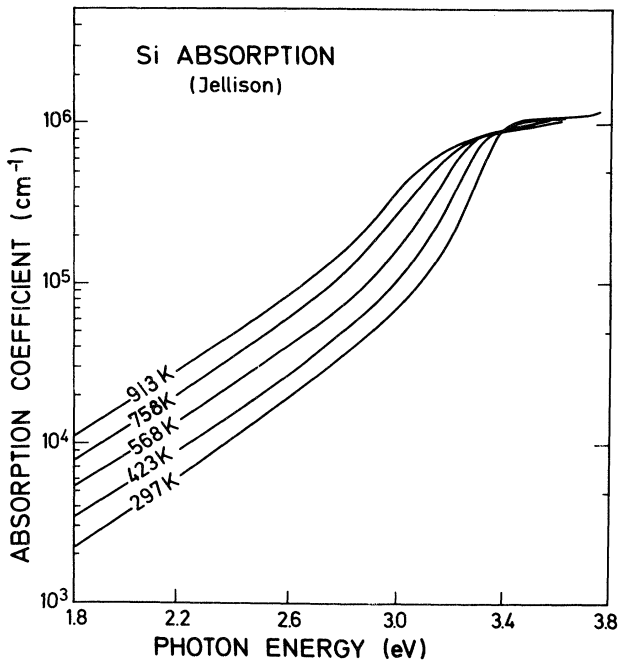

FIG. 2. Si absorption coefficients used for correcting the Raman data. Curves are based on the data of Ref. 7 and in some cases are interpolated between measured temperatures.

Raman susceptibility χ_S'' is then related to R_S' via the transmission factor (T_ST_L), the index of refraction factor $(\eta_L\eta_S)^{-1}$, and the absorption coefficient factor $(\alpha_L+\alpha_S)^{-1}$ [see Eq. (4)]. It is important to recognize that these effects are not only frequency dependent near the resonance but also temperature dependent since the resonance shifts and broadens with temperature. The recent ellipsometric measurements of the Si optical constants over a range of temperature[7] afford an unusual opportunity to apply these corrections with a high degree of confidence. Figures 1(a) and 1(b) show the variation of transmission coefficients and the index of refraction for several temperatures. These curves have been calculated

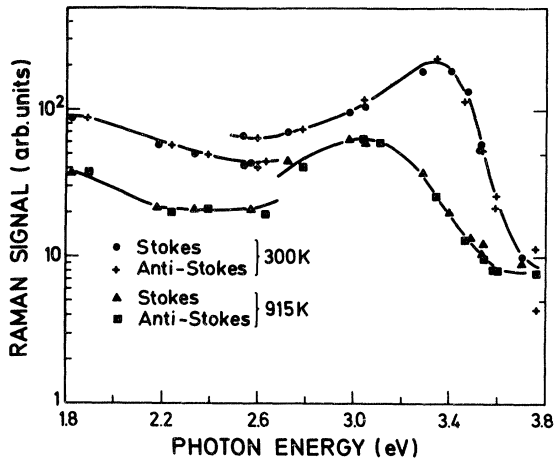

FIG. 3. Raman photon-counting rate arbitrarily normalized and corrected only for relative efficiency of the collection system. Anti-Stokes data have been multiplied by $\exp(\hbar\omega_0/kT)$. Breaks in curves occur where incident laser polarization was changed.

from the data of Ref. 7. Figure 1(c) shows the net correction due to these effects. The data shown are appropriate for the polarization used in each region. (The discontinuity arises solely from the polarization-dependent reflectivity of the incident laser beam.) The observed count rate must be *divided* by these values so that the minima observed above 3.0 eV tend to *enhance* the observed resonance in χ_S'' in this region.

By far the largest correction arises from the scattering volume effect, i.e., $[\alpha_S+\alpha_L(1-\eta_L^{-2}\sin^2 45°)^{-1/2}]^{-1}$, which is thus coupled to η_L. However, neglecting the entire factor $(1-\eta_L^{-2}\sin^2 45°)^{-1/2}$ produces an error of less than 2% throughout the spectral region of interest, and therefore we drop it completely. The absorption coefficients used for this correction are shown in Fig. 2. These curves have been obtained from the data of Jellison and Modine[7] with linear interpolations used to obtain the curves at higher temperatures. In all cases these elevated temperatures lie *between* temperatures for which data were reported in Ref. 7.

RESONANCE RAMAN ENHANCEMENTS

Stokes and anti-Stokes Raman signals were observed with thirteen cw argon- and krypton-ion laser lines and at twice the frequency of the 752.5 nm Kr line. Frequency doubling was performed by focusing the ~2-W output at 7525 Å in an angle-tuned $LiIO_3$ crystal yielding ~0.35 mW of 3762.5-Å power at the sample after separation from the fundamental in a prism spectrometer. The Raman signal at the highest and lowest temperatures are plotted in Fig. 3. Count rates have been adjusted only for relative collection efficiency. The discontinuity in the curve arises from a change in laser polarization and the resulting change in the transmission coefficient T_L. We chose to maximize spectrometer efficiency by obtaining vertical scattered polarization in the (2.6—3.8)-eV region and horizontal polarization at lower frequencies. For the (100) sample with [010] vertical this required incident polarization perpendicular (parallel) to the horizontal scattering plane for the (1.8—2.6)-eV [(2.6—3.8)-eV] region.

The raw signal clearly shows the presence of the resonance at the direct gap and its shift and broadening with temperature. However, the amplitude of the resonance enhancement is not impressive especially when one recalls the ω^3 dependence which itself gives a slow rise with increasing frequency. It must be remembered, on the other hand, that the several corrections discussed above tend to suppress the real resonance which is occurring in the Raman susceptibility. When these effects are removed, we find a very strong resonance in the susceptibility at all temperatures.

Figure 4 shows the square of the Raman susceptibility observed at room temperature. The data show a remarkably strong resonance of more than 3.5 decades. In addition we display two calculated curves of $|d\epsilon/d\omega|^2$. The dashed curve was obtained from ellipsometric measurements on the same sample which had been used for the Raman work.[12] (A nearly identical curve was obtained from a portion of the same Si wafer which had not undergone the repeated temperature cycling of the Raman measurements. This result indicates that the sample surface oxide conditions were stable through the course of the Raman measurements.) The solid curve indicates Jellison's calculation[13] of the same quantity from his ellipsometric measurements.[7] The slight differences between the two ellipsometric results may arise from minor differences in sample surface conditions and/or the density of points digitized before data analysis.

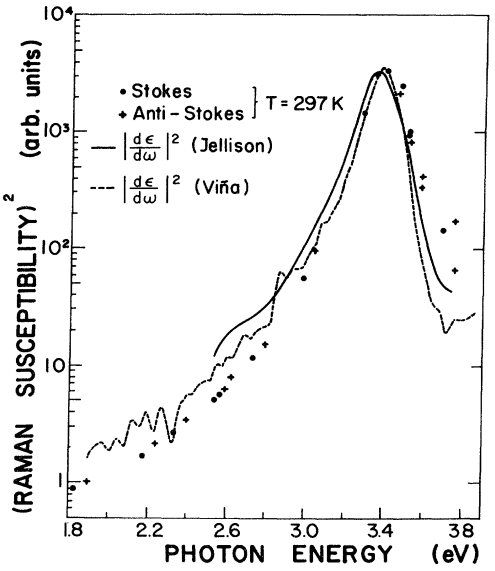

FIG. 4. Room-temperature Raman susceptibility squared from both Stokes and anti-Stokes data compared with data for $|d\epsilon/d\omega|^2$ from Jellison (Ref. 13) and similar data obtained by Viña (Ref. 12) from the sample used for the Raman measurements.

Both sets of ellipsometric data have been shifted to higher frequency by 32 meV, i.e., one half of the optic-phonon energy. The physical origin of such a shift is treated in the discussion section. With this shift the agreement between the Raman susceptibility χ_S'' and $|d\epsilon/d\omega|$ is remarkable since only one overall multiplica-

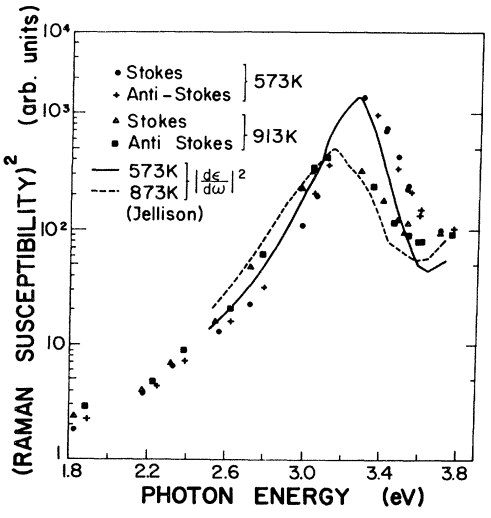

FIG. 5. Raman susceptibility squared (data points) at two elevated temperatures and $|d\epsilon/d\omega|^2$ (curves) from Jellison (Ref. 13) for similar temperatures.

tive constant was adjustable. Note also that the anti-Stokes data (plotted one phonon energy higher than the Stokes data) fall on the same resonance curve as expected from time reversal invariance.

Figure 5 shows the Raman susceptibility squared at two elevated temperatures together with Jellison's results[13] for $|d\epsilon/d\omega|^2$ at closely corresponding temperatures. Again the agreement is pleasing when the ellipsometric results are shifted higher by one half the optic-phonon energy. It should be noted, however, that even after this upward shift, the $|d\epsilon/d\omega|^2$ curves at these higher temperatures appear to lie systematically lower than the Raman data. [Note that the apparently better fit to the 913-K Raman data arises from the lower temperature (873 K) of the $|d\epsilon/d\omega|^2$ data.] Nevertheless the agreement is satisfying because the same multiplicative constant (vertical shift) has been used to compare all three Raman and ellipsometric results of Figs. 4 and 5.

The largest discrepancy between the Raman data and the ellipsometric $|d\epsilon/d\omega|^2$ occurs above the resonance where for all three temperatures $|d\epsilon/d\omega|^2$ shows a larger dip than the Raman susceptibility. However, this may arise from contributions to the Raman strength from the incipient E_2 resonance at 4.5 eV at room temperature. The enhanced Raman signal above 3.6 eV would then be explained by stronger electron-phonon coupling to the states involved in the E_2 resonance.

For the Raman data taken with sample temperatures of 423 and 758 K, corresponding measurements of $|d\epsilon/d\omega|^2$ are not available. Thus we show in Fig. 6 these data with smooth curves visually drawn through the measured points. Although the vertical scale in Figs. 4–6 is indicated as relative, the differences among the results at the respective temperatures are meaningful. Thus the peak height of the resonance drops by a factor of 7.7 ± 0.5 as the sample temperature is raised from 297 to 913 K. This drop in peak height is closely related to the increase in width of the resonance which is also clearly evident (see next section).

One overall scale factor for all of the data therefore determines the absolute Raman susceptibility. This overall calibration may be obtained from the results of Grimsditch and Cardona,[14] who have found the allowed component of the Raman tensor to be $a=+60\pm20$ Å^2 at $\hbar\omega_L=1.9$ eV. In terms of the Raman susceptibility, a for the zone center optic mode of Si is given by

$$a=\tfrac{1}{2}V_c\frac{d\chi_{12}}{du_3}=\frac{1}{2\sqrt{2}}(V_cM)^{1/2}\frac{d\chi'_{12}}{d\xi_3}\ , \qquad (6)$$

where V_c is the volume of the primitive cell, $2u$ is the relative sublattice displacement, and M is the Si atomic mass.

The shift of the resonance peak with temperature and the increasing width are plotted in Fig. 7 together with similar data from ellipsometric measurements of Jellison.[13] The Raman data indicate a linear shift of the resonance (i.e., the E'_0,E_1 gap) of -3.7×10^{-4} eV/K over the entire temperature range. The shift indicated by the ellipsometric data ($|d\epsilon/d\omega|^2$) is the same within experimental error. This agreement in the shifts is in contrast with previous reports indicating that the Raman resonance in, e.g., InAs (Ref. 15) and Ge-Si alloys[16] decreased much more slowly with increasing temperature than did

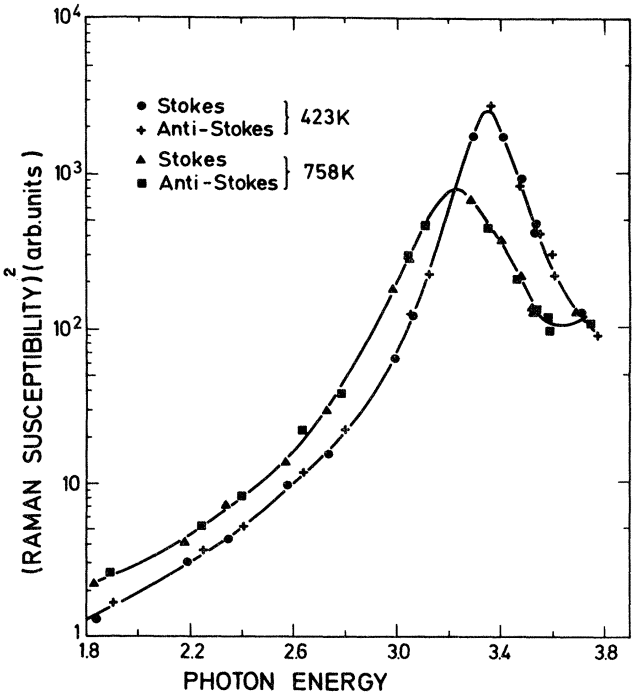

FIG. 6. Raman susceptibility squared for two additional temperatures with smooth curves visually drawn to fit. Appropriate $|d\epsilon/d\omega|^2$ data not available.

the peak in the optical functions. The present data, however, extend over a much wider temperature range than previous studies and furthermore have the advantage of the availability of more extensive optical constant data for making the necessary corrections. Therefore, we believe the earlier data should be reexamined in view of the present results.

Allen and Cardona[8] have recently calculated the temperature dependence of the E'_0 gap in Si due to electron-

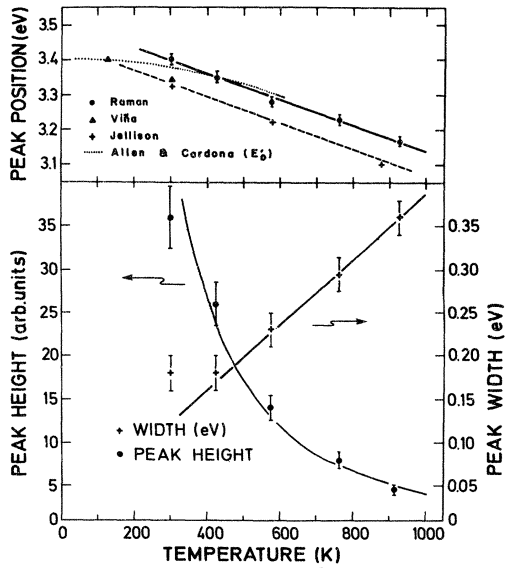

FIG. 7. Position, height, and width of the Raman susceptibility resonance peak vs temperature. Dashed curve shows the temperature shift of the E'_0 gap calculated by Allen and Cardona (Ref. 8). Solid curves are visual fits for the width $\sim T$ and height $\sim T^{-2}$.

phonon interactions. The effect due to thermal expansion must be added to their calculated shift at constant volume. This is related to the bulk modulus B and the linear expansion coefficient α via[8]

$$\left[\frac{\partial E_g}{\partial T}\right]_{\text{th expan}} = 3B\alpha\left[\frac{\partial E_g}{\partial P}\right]_V \cong -0.48\times 10^{-4} \quad (7)$$

$$(300 < T < 600\ \text{K})$$

(in units of eV/K), where we have used values from Ref. 11. The results of Ref. 8 with this additional term included are shown as the dotted line in Fig. 7. The calculation was done only for $T \leq 600$ K, but in the 300-K region of overlap the observed shift is considerably larger than the calculated values. This may arise from the fact that the Raman susceptibility, as well as the optical constants, is primarily influenced by the much higher density of states for the E_1 gap than for the E_0' gap at Γ for which the calculations[8] were performed.

We should note here that the temperature shift of the peak in ϵ_1 near 3.4 eV as shown by Jellison (Ref. 7, Fig. 4) is considerably larger at high temperatures 600–900 K ($\sim -4.8\times 10^{-4}$ eV/K) than we find here. However, the shift in the peak of ϵ_1 (real part) does not give directly the shift of the band gap since it is influenced by increased broadening with temperature. This shift is better identified via spectral derivatives as discussed by Viña and Cardona.[12] This is just the motivation behind our use of $|\chi_S''|^2$ and $|d\epsilon/d\omega|^2$ for the results shown in Fig. 7.

RAMAN SUSCEPTIBILITY: CLASSICAL vs QUANTUM

The classical and quantum descriptions of the Raman susceptibility χ_S'' have been discussed in detail by Cardona.[1] Here we only summarize the results in order to discuss more carefully our upward displacement by one half the phonon energy of the $|d\epsilon/d\omega|^2$ curves in Figs. 4 and 5. This comparison also provides a useful basis for analysis of the temperature dependence of the Raman resonance position, width and height.

The usual classical expression for the susceptibility near an isolated resonance ω_0 is

$$\chi(\omega) \sim \frac{F}{\omega_0^2 - \omega^2 - i\omega\gamma}\ . \quad (8)$$

One readily obtains from this the Raman susceptibility

$$\chi_S'' = \frac{d\chi'}{d\xi} \sim \frac{2\omega_0 F}{(\omega_0^2-\omega_L^2-i\omega\gamma)^2}\frac{d\omega_0}{d\xi} + \frac{1}{\omega_0^2-\omega_L^2-i\omega\gamma}\frac{dF}{d\xi}\ , \quad (9)$$

where F is the oscillator strength tensor. Here the prime on $d\chi'/d\xi$ is a reminder that the susceptibility has been renormalized appropriately to keep the derivative with respect to the normal mode coordinate ξ volume independent (cf. Ref. 1). (Again, we have for convenience suppressed the tensor character of χ', χ_S'', and F.) The first term of Eq. (9) represents contributions arising from the shift of the transition energy ω_0 due to the phonon. The second term results from perturbations of the oscillator strength tensor due to mixing of states by the phonon.

The corresponding quantum description can be written via third-order perturbation theory and has the form[1,9]

$$\chi_S'' \sim \sum_{i,j} \frac{\langle 0|H_{e\text{-}R}|i\rangle\langle i|H_{e\text{-ph}}|j\rangle\langle j|H_{e\text{-}R}|0\rangle}{(\omega_{j0}-\omega_L+i\Gamma_j)(\omega_{i0}-\omega_S+i\Gamma_i)} + \cdots\ . \quad (10)$$

Here ω_{j0} and ω_{i0} are the transition energies corresponding to ground state 0 and intermediate states i and j. $H_{e\text{-}R}$ and $H_{e\text{-ph}}$ are the interaction Hamiltonians of the electron-radiation field and electron-phonon coupling, respectively.

The first term of Eq. (9) arises from the "two-band" contributions of Eq. (10)—that is, terms with $i=j$ so that only two bands, 0 and i, contribute. The second, less strongly resonant, term of Eq. (9) arises from "three-band" contributions to Eq. (10)—i.e., those with $i\neq j$. [The unspecified nonresonant terms included in the ellipsis of Eq. (10) arise from the five other time orderings of the three interactions in the perturbation treatment.]

The quantum expression is distinguished from the classical one by the explicit display of an "outgoing resonance," $\omega_S=\omega_{i0}$, as well as the usual "incoming resonance," $\omega_L=\omega_{j0}$. For most three-band contributions one of the denominators is usually far from resonance and two distinct resonances occur, one at ω_L and one at ω_S. In this case if the width of the electronic resonance is large compared with the phonon energy ($\Gamma \gg \omega_L-\omega_S$) the Raman susceptibility will peak halfway between ω_L and ω_S. Then the Raman susceptibility should appear much like the classical expression [second term in Eq. (9)], except that the peak in χ_S'' would be shifted upward by one half the phonon energy, $\omega_0/2$, from the peak in $|d\epsilon/d\omega|^2$.

At the E_0', E_1 gap of Si, however, Renucci *et al.*[2] have shown that the resonance behavior has the structure entirely of a two-band resonance. This is a consequence of the fact that the major three-band term behaves like a two-band resonance due to the small spin-orbit splitting of the valence band ($\Delta \simeq 0.03$ eV) compared with the width of the resonance ($\Gamma \simeq 0.1$ eV at room temperature). In this approximation we may set $\omega_{j0}=\omega_{i0}$ and $\Gamma_j=\Gamma_i$, and the similarity of the quantum expression Eq. (10) now appears with the first term of the classical formula [Eq. (9)], except that qualitatively the resonance peak is again upshifted halfway between ω_L and ω_S.

SHAPE OF THE RESONANCE

The structure of the resonance at the E_1 gap in Si is that essentially of a two-dimensional (2D) critical point. (The contribution of the nearly degenerate E_0' gap at Γ is expected to be much smaller because of the much lower density of states associated with these transitions.) For such a 2d resonance, Eq. (10) [and implicitly Eq. (9) also] must be integrated over the appropriate joint density of electronic states participating in the transition.

If the small spin-orbit splitting Δ is neglected, the density of states for conduction- to valence-band transitions, ω_{cv}, is[1]

$$\rho_d(\omega_{cv})=\frac{\Delta k}{\pi}m_d\Theta(\omega_{cv}-\omega_1) \tag{11}$$

where Δk is the length of k space over which the conduction and valence bands are parallel ($m_{||}^*=\infty$), m_d is the density of states effective mass in the transverse direction, ω_1 is the position of the E_1 gap and $\Theta(\omega_{cv}-\omega_1)$ is the unit step function.

In the limit of large broadening, $\Gamma \gg \Delta$ and $\Gamma \gg \omega_L-\omega_S$, the integration of Eq. (10) over the density of states yields directly

$$\chi_S''\sim(\omega_1+\omega_0/2-\omega_L+i\Gamma_1)^{-1}\,, \tag{12}$$

where we have explicitly included the shift of $\omega_0/2$ discussed above. Finally we obtain for the most strongly resonant term at the E_1 gap

$$\chi_S''^*\chi_S''\sim\{[(\omega_1+\omega_0/2)-\omega_L]^2+\Gamma_1^2\}^{-1}\,. \tag{13}$$

Thus in the large damping limit, which is clearly satisfied at temperatures above ambient, we expect that the amplitude of the resonance should be proportional to Γ_1^{-2}. The data of Fig. 7 are in good agreement with this expectation thus adding additional support to the identification of the E_1 gap in Si as a two-dimensional critical point.

The width Γ and shift $\Delta\omega_0$ with temperature are complementary (imaginary and real) terms of the electron self-energy due to phonon interaction. The width and shift are sensitive to different parts of the phonon spectrum;[8] however, in the limit of high temperatures ($T>\hbar\omega_0/k=500\,^\circ$C) both should become linear in T since the phonon population itself is linear in T.

The shift of the peak position has an additional term due to thermal expansion but at high temperatures it also is linear in T. Figure 7 clearly shows this linear shift with increasing temperature for the entire range 300–915 K. The increase in width, however, is proportional to T only above $\sim$600 K. We believe this arises from the intrinsic width of the resonance due to the combination of E_0' and E_1 critical points, the neglect of spin-orbit splitting, and the assumption that $\omega_L\approx\omega_S$ in the above discussion. The high-temperature trends, however, provide clear evidence that the resonance behavior of the Raman susceptibility is well understood in the present theoretical framework.

STOKES- TO ANTI-STOKES-INTENSITY RATIOS

From Eq. (5) we readily obtain the Stokes- to anti-Stokes-intensity ratio of counting rates outside the sample as

$$\frac{R_S'}{R_{AS}'}=\frac{T_S(\alpha_{AS}+\alpha_L)\eta_{AS}\omega_S^3}{T_{AS}(\alpha_S+\alpha_L)\eta_S\omega_{AS}^3}\,\frac{|\chi_S'|^2}{|\chi_{AS}'|^2}\,\frac{n(\omega_0)+1}{n(\omega_0)}\,. \tag{14}$$

In thermal equilibrium, the last (phonon occupation) factor becomes simply $\exp(\hbar\omega_0/kT)$. Equation (14) thus forms the basis of temperature measurements from the Stokes- to anti-Stokes-intensity ratio. The temperature inference must be made with care since, as seen above, all of the factors except for ω^3 are themselves temperature dependent. We have seen that the absorption factor and the Raman susceptibility factor are by far the most strongly resonant and thus most strongly dependent on temperature. This was recognized in the first pulsed Raman measurements of Lo and Compaan,[4] where it was argued, however, that the net temperature-dependent correction would be small for frequencies well below the direct gap.

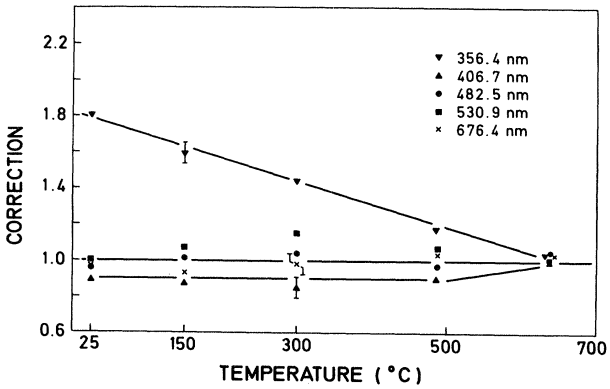

FIG. 8. Temperature dependence of the total correction factor needed to extract a phonon population ratio $[n(\omega_1)+1]/n(\omega_0)$ from Stokes- to anti-Stokes-intensity ratios for several laser frequencies. Typical error of ±5% is shown.

In Fig. 8 we show the temperature dependence of the corrections by plotting $(\omega_S/\omega_{AS})^3\exp(\hbar\omega_0/kT)$ divided by the Stokes- to anti-Stokes-intensity ratio for several of the laser lines in this study. It is clearly seen that the correction factors for frequencies below the resonance are very close to unity and essentially temperature independent. This confirms the behavior predicted in Ref. 4 and arises from the compensating spectral dependence of the absorption correction and of the Raman susceptibility corrections. For frequencies slightly above the resonance, however, the correction factor varies considerably with temperature. This arises from the fact that the absorption coefficient is approximately independent of frequency but the Raman susceptibility is rapidly decreasing with frequency in this spectral region. This behavior and its importance for pulsed Raman measurements of temperature during laser annealing is discussed more fully in Refs. 17 and 18.

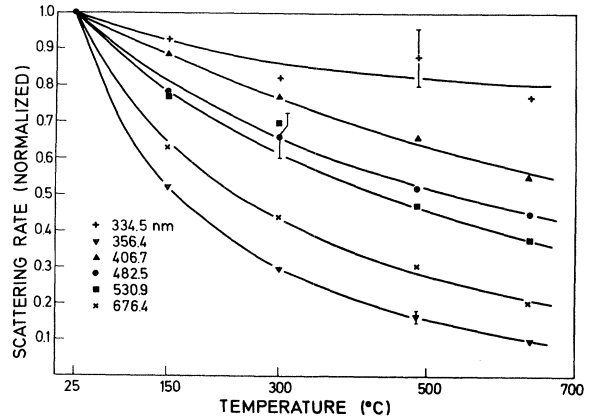

FIG. 9. Temperature dependence of the observed Stokes count rate for several laser lines. Smooth curves are visual fits to the data. Typical error of ±10% is shown for several points.

RAMAN SCATTERING RATE VS TEMPERATURE

Although the Raman susceptibility falls rapidly with increasing temperature in the region from 3.4 to 3.6 eV, the data of Fig. 6 show that the susceptibility increases with temperature for frequencies below ~ 3.2 eV. This is of course the expected behavior of a resonance which broadens and shifts with temperature. The Raman susceptibility, however, does not give directly the behavior of the Raman signal (photon scattering rate) because of the various corrections. The raw data of Fig. 3 show that the Raman signal actually decreases with temperature at all frequencies. In Fig. 9 we display for several laser lines the variation of Raman signal with crystal temperature. The behavior is clearly a strong function of laser frequency.

For frequencies at or just above the resonance at room temperature, e.g., 356.4 nm, the decrease is largely due to the shift of the resonance with temperature. Well below the resonance, e.g., 676.4 nm, the decrease is largely a result of increasing absorption with temperature. Just below the room-temperature resonance peak, e.g., 406.7 and 482.5 nm, the fall in scattering rate is less because the approaching resonance tends to compensate for the increasing absorption as temperature rises. Finally at 334.5 nm the combined influence of both the E_0', E_1 resonance and the E_2 resonance apparently tends to stabilize the intensity.

It is interesting in this respect to examine the intensity dependence of the pulsed Raman measurements[4,5] of lattice temperature as inferred from Stokes- to anti-Stokes-intensity ratios. The studies by Compaan *et al.*[4] at 405 nm and by von der Linde *et al.*[5] at 532 and 355 nm all show significant reductions in signal as the heat fluence increases. Comparison with the data of Fig. 9, however, shows that this drop is quite consistent in all cases with the inferred temperatures (300—450 °C) in these experiments.

CONCLUSIONS

The results of this study show clearly that for the E_0', E_1 gap in the Si the Raman susceptibility χ_S'' is represented remarkably well by the frequency derivative of the dielectric constant $|d\epsilon/d\omega|$, provided the latter is shifted higher by approximately one half the phonon frequency. The data presented here remove some ambiguities which remained from a previous study[2] regarding the resonance structure and position at room temperature. The shift and broadening of the resonance with temperature fit the classical model (quasistatic approximation) very well. The drop in peak height of the resonance with temperature can be understood when details of the band structure (i.e., the fact that the E_1 gap arises from a 2D critical point) are applied to the intermediate electronic states. Anti-Stokes data fall on the same curve as the Stokes data, confirming the validity of time-reversal invariance in the Raman process.

We have also included data here on the temperature dependence of correction factors to be used for inferring zone-center optic-phonon populations from anti-Stokes- to Stokes-intensity ratios. Finally we have presented the temperature dependence of the Raman signal at a variety of wavelengths. Both of the above results are readily understood in terms of the temperature dependence of the optical constants and the shift and broadening of the resonance in the Raman susceptibility.

Note added in proof. After submission of this manuscript, a related study appeared which compares the earlier room-temperature Raman measurements (Ref. 2) with new data on $|d\epsilon/d\omega|$ (actually the same data we have used here). See G. E. Jellison, Jr., D. H. Lowndes, and R. F. Wood, Phys. Rev. B 28, 3272 (1983). These authors obtain a larger shift of the E_1 gap with temperature. (See the last paragraph of the section Resonance Raman Enhancements above.) And they do not include the $\omega_0/2$ displacement between $|\chi_S''|^2$ and $|d\epsilon/d\omega|^2$ which we find to be necessary. These two factors account for most of the differences in conclusions between the two studies as they relate particularly to temperature-dependent corrections to the Raman Stokes- to anti-Stokes-intensity ratio.

ACKNOWLEDGMENTS

The authors are indebted to M. Cardona for making this work possible during their rather brief residences at the Max-Planck Institute and for many illuminating discussions during the course of this work. We are grateful to G. E. Jellison for making available to us his calculated results for $d\epsilon/d\omega$ prior to publication. The help of J. Kuhl for the frequency doubling and of L. Viña and C. Umbach in the ellipsometric measurements and analyses was essential and is deeply appreciated. One of the authors (A.C.) thanks the A. von Humboldt Foundation for fellowship support during this work. Finally, the expert technical assistance of P. Wurster, H. Hirt, and M. Siemers greatly facilitated this work.

---

*On sabbatical leave from Department of Physics, Kansas State University, Manhattan, KS 66506 (permanent address).

†On sabbatical leave from Department of Physics, Victoria University, Wellington, New Zealand (permanent address).

[1]Resonance Raman scattering in semiconductors is reviewed in detail most recently by M. Cardona, in *Light Scattering in Solids II,* Vol. 50 of *Topics in Applied Physics,* edited by M. Cardona and G. Güntherodt (Springer, Berlin, 1982).

[2]J. B. Renucci, R. N. Tyte, and M. Cardona, Phys. Rev. B 11, 5885 (1975).

[3]See, for example, *Laser-Solid Interactions and Transient Thermal Processing of Materials,* edited by J. Narayan, W. L. Brown, and R. A. Lemons (North-Holland, New York, 1983).

[4]H. W. Lo and A. Compaan, Phys. Rev. Lett. 44, 1604 (1980).

[5]A. Compaan, H. W. Lo, M. C. Lee, and A. Aydinli, Phys. Rev. B 26, 1079 (1982); A. Compaan, in *Cohesive Properties of Semiconductors under Laser Irradiation,* edited by L. Laude (Martinus Nijhoff, The Hague, 1983), p. 404; A. Compaan, H. W. Lo, A. Aydinli, and M. C. Lee, in *Laser-Solid Interactions and Transient Thermal Processing of Materials,* Ref. 3, p. 23.

[6]D. von der Linde and G. Wartman, Appl. Phys. Lett. 41, 700 (1982); D. von der Linde, G. Wartman, and A. Ozols, in *Laser-Solid Interactions and Transient Thermal Processing of Materials,* Ref. 3, p. 17.

[7]G. E. Jellison, Jr., and F. A. Modine, Appl. Phys. Lett. 41, 180 (1982); Phys. Rev. B 27, 7466 (1983).

[8]P. B. Allen and M. Cardona, Phys. Rev. B 27, 4760 (1983).

[9]W, Hayes and R. Loudon, *Scattering of Light by Crystals* (Wiley, New York, 1973).

[10]A. Compaan, A. Z. Genack, H. Z. Cummins, and M. Washington, in *Light Scattering in Solids,* edited by M. Balkanski, R. C. C. Leite, and S. P. S. Porto (Flammarion, Paris, 1975), p. 39.

[11]*Landolt Börnstein: Physics of Group IV Elements and III-V Compounds,* edited by O. Madelung (Springer, Berlin, 1982), Group II, Vol. 17a.

[12]These measurements were performed by L. Viña and C. Umbach. The ellipsometer is described by L. Viña and M. Cardona in *Proceedings of the 16th International Conference on the Physics of Semiconductors,* edited by M. Averous (North-Holland, Amsterdam, 1983), p. 356. The absorption data of W. C. Dash and R. Newman [Phys. Rev. 99, 1151 (1955)] have been used for the imaginary part of the dielectric constant ϵ_2 below 2.6 eV.

[13]G. E. Jellison, Jr. (private communication).

[14]M. Grimsditch and M. Cardona, Phys. Status Solidi B 102, 155 (1980).

[15]M. A. Renucci, J. B. Renucci, and M. Cardona, Phys. Status Solidi B 49, 625 (1972).

[16]M. A. Renucci, J. B. Renucci, and M. Cardona, in *Light Scattering in Solids,* edited by M. Balkanski, R. C. C. Leite, and S. P. S. Porto (Flammarion, Paris, 1975), p. 326.

[17]A. Compaan, M. C. Lee, H. W. Lo, G. J. Trott, and A. Aydinli, J. Appl. Phys. 54, 5950 (1983).

[18]G. Wartman, D. von der Linde, and A. Compaan, Appl. Phys. Lett. 43, 613 (1983).